Polymer 311 (2024) 127536

Contents lists available at ScienceDirect

Polymer

journal homepage: www.elsevier.com/locate/polymer

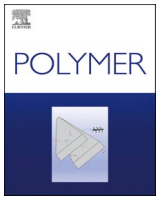

Fumasep FAA-3-PK-130: Exploiting multinuclear solid-state NMR to shed light on undisclosed structural properties

Andrea Giovanelli [a], Alfonso Pozio [b], Andrea Pucci [a,c], Marco Geppi [a,c,*], Francesca Martini [a,c]

[a] Department of Chemistry and Industrial Chemistry, University of Pisa, Via G. Moruzzi 13, 56124, Pisa, Italy
[b] ENEA, C.R. Casaccia, Via Anguillarese 301, 00123, Rome, Italy
[c] CISUP, Center for Instrument Sharing, University of Pisa, Lungarno Pacinotti 43, 56126, Pisa, Italy

ARTICLE INFO

Keywords:
^{13}C CP-MAS
Spin-lattice relaxation
Anion exchange membranes
^{2}H NMR
Ion channels
Water mobility

ABSTRACT

Fumasep FAA-3-PK-130 is considered the state-of-the-art among the different commercially available Anion Exchange Membranes (AEMs). It is produced by Fumatech GmbH as a cost-effective blend of polyetheretherketone (PEEK) and poly (phenylene oxide) (PPO) characterized by high hydroxyl ions conductivity, high thermal and chemical resistance, and high dimensional stability. Nevertheless, the chemical structure of the anion exchange sites and their contents were unknown so far.

In this paper, we report a detailed structural characterization of Fumasep FAA-3-PK-130 to identify the material phase composition, the nature of the conducting moieties and their interactions with the adsorbed water molecules. A complete phase segregation between PPO and PEEK was found on a micrometric scale from ^{1}H spin-lattice relaxation times and micro-ATR analysis. Multinuclear (^{1}H, ^{13}C, ^{19}F) Solid-State NMR spectra, combined with nuclear spin relaxation measurements, allowed us to identify the anion exchange moiety with benzyl-ethyl-dimethylammonium. This is present as functionalizing group of PPO monomers with a functionalization degree of about 40 %. Moreover, the mobility of water absorbed in the membrane was studied by ^{2}H Solid-State NMR on samples hydrated with deuterated water under controlled relative humidity: at low relative moisture, two different types of environments were found for water molecules, compatible with two types of water-ion clusters, one of which contains water molecules with a restricted mobility, limited to C_2 jumps, due to strong interactions with ions.

1. Introduction

The quest to produce cheap and green hydrogen requires the optimization of new methods that can reduce costs while working with renewable energy sources. Among different technologies, Anion Exchange Membranes-Water Electrolysers (AEMs-WE) are promising candidates for this application because they employ a polymeric membrane with high tunability of properties and allow the usage of cheap transition metal catalysts.

AEMs for water electrolysis consist of polymeric membranes bearing positively charged groups either on the macromolecular backbone or sidechains. Such elements allow the closure of the electrolyser chemical circuit with anions, usually hydroxyl groups that diffuse from the cathode to the anode, while acting as an electric insulator and preventing hydrogen crossover. Moreover, the membrane must have good thermal and chemical resistance in the working environment that is characterised by temperatures reaching 100 °C and high pH [1,2]. The most used cationic moieties in AEMs are ammonium groups, usually obtained via tertiary amine quaternization with alkyl halides. These groups are of extreme relevance because they offer a wide structural variability to modulate membrane ion conductivity and durability [3]. The main issue with ammonium groups lies in the low chemical resistance in the working environment due to the Hoffmann elimination and nucleophilic substitution caused by the alkaline environment [4].

In the literature, different polymeric backbones have been used to obtain AEMs. Some examples include polyketone (PK) [5], polyetheretherketone (PEEK) [6], poly (aryl ether sulfone) (PAES) [7] and poly (phenylene oxide) (PPO) [8,9]. PPO constitutes the backbone of FAA-3, an ionomer commercialized by Fumatech BWT GmbH as a solution in NMP (Fumion) or as a membrane (Fumasep) [10]. The ion conductivity of FAA-3 is given by quaternary ammonium groups bound to the main polymeric backbone. However, the structure of the

* Corresponding author. Department of Chemistry and Industrial Chemistry, University of Pisa, Via G. Moruzzi 13, 56124, Pisa, Italy.
E-mail address: marco.geppi@unipi.it (M. Geppi).

https://doi.org/10.1016/j.polymer.2024.127536
Received 19 June 2024; Received in revised form 10 August 2024; Accepted 22 August 2024
Available online 23 August 2024

ammonium group has not been disclosed yet [11]. Fumasep FAA-3-PK-130 membrane incorporates FAA-3 as the ionomer and PEEK as the supporting polymer matrix, enhancing mechanical properties and mitigating swelling during water adsorption [12]. Given the superior performance of the Fumasep FAA-3-PK-130 membrane in terms of conductivity, durability, and cost-effectiveness, it has become a benchmark for evaluating new AEMs [13,14]. Despite these well-documented benefits, the exact nature of its phase separation and structural composition remains largely unexplored. Furthermore, FAA-3 solutions are extensively utilized to create anion-conductive composite materials with improved mechanical and chemical stability [15–17].

In the field of material research, it is essential to characterise properties in conditions that are representative of the application environment. When dealing with polymers, many different techniques can be applied, but among them, Solid-State NMR (SSNMR) has established as a golden standard because of the wide range of physical properties that can be investigated and the high level of detail of the achieved information [18]. Some examples are phase separation [19,20], structural and conformational properties [21,22], backbone [23,24] and sidechain [25,26] dynamics and molecule-polymer interactions [27].

Notably, when dealing with ion exchange membranes (IEMs), SSNMR can be used to unravel additional features that are usually difficult to gather using traditional techniques. For example, ions diffusion within the membrane can be studied by observing a nucleus of the diffusing molecule under the effect of magnetic field gradients. This approach has been widely used to measure ion diffusivity in polymer electrolytes [23,28] as well as IEMs, as in the cases of Nafion [29,30] and FAA-3 [31], but also to determine the structure of novel anion exchange fuel cell membranes [32].

Another property strictly related to diffusivity, of particular interest in IEMs, is the formation of ionic channels upon water adsorption. This phenomenon has been deeply studied in the case of Nafion [33,34] by neutron scattering [35], small angles x-ray diffraction (SAXS) [35] and atomic force microscopy (AFM) [36]. For example, in the case of FAA-3-PK-130 in bromide form, Barnes et al. highlighted the formation of ionic channels by using AFM after hydration with a relative humidity (RH) of at least 80 % [36]. Chikvaidze et al. proposed using micro Raman spectroscopy to study FAA-3-PK-130 in dry and humid conditions to determine *O*–H vibrations under different conditions [37]. However, the broadening of the molecular vibration peaks makes it challenging to attribute all signals accurately.

Therefore, this study aims to elucidate the detailed composition and microstructural properties of the Fumasep FAA-3-PK-130 membrane. The central hypothesis posits that a comprehensive understanding of its phase separation and structural characteristics will reveal the underlying mechanisms contributing to its high performance. Notably, we present a multinuclear SSNMR characterisation of Fumasep FAA-3-PK-130. Different nuclei (^{1}H, ^{13}C, ^{19}F) have been used to identify the nature of the ion conductive moieties, the constituting polymers and to understand their phase separation within the membrane. Moreover, the structure of the undisclosed functionalizing ammonium group, its location, and the functionalization degree have been determined using quantitative ^{13}C spectra and ^{13}C spin-lattice relaxation times. The membrane has been studied in ambient conditions and after hydration with deuterated water under controlled RH. Static ^{2}H NMR spectra have been recorded on the hydrated material to monitor the presence of ionic channels from deuterium line shape analysis. This knowledge is anticipated to provide valuable insights for the development of next-generation AEMs with optimized properties for a wide range of industrial applications. By addressing these gaps, the research seeks to advance the field of membrane technology and enable the engineering of more efficient and robust materials.

2. Experimental part

2.1. Materials

Fumasep FAA-3-PK-130 has been provided by Fumatech BWT GmbH. The membrane was washed with deionised water and then dried in an oven at 50 °C overnight before use.

The controlled hydration was performed according to the procedure reported by Greenspan et al. [38] using saturated solutions of KCl and LiBr in D_2O. Before the hydration, the membrane was dried under vacuum (≈4 mbar) at 50 °C for 5 h. The hydration was carried out over one week at 25 °C.

D_2O with 99.9 % deuterium content was purchased from Sigma-Aldrich. KCl (Sigma-Aldrich) and LiBr (Sigma-Aldrich) were dried under vacuum with a heat gun.

2.2. Characterization techniques

Solid-State NMR experiments were performed on a Bruker Avance Neo spectrometer operating at the ^{1}H Larmor frequency of 500.13 MHz. A two-channel CP-MAS probe that supports rotors (made of zirconia and closed with Vespel® caps) with an outer diameter of 4 mm was used. Chemical shift absolute referencing, based on the ^{13}C spectrum of adamantane, was used [39]. Unless otherwise stated, all spectra were recorded at 298 K under Magic Angle Spinning (MAS) using a spinning frequency of 15 kHz. The 90° pulse durations were 4.3, 3.7, 4.1, and 6 μs for ^{1}H, ^{19}F, ^{13}C, and ^{2}H, respectively. ^{1}H spectra were recorded using 40 scans and different recycle delays, from 1 to 30 s ^{19}F MAS spectra were recorded using 16 scans and a recycle delay of 10 s ^{13}C Direct Excitation (DE) spectra were recorded using 16000 scans and recycle delay of 2 s ^{1}H–^{13}C cross polarization (CP) and heteronuclear correlation (HETCOR) spectra were acquired using a linear ramped-amplitude CP scheme on ^{1}H nuclei with a SPINAL [40] high-power decoupling scheme during acquisition. A contact time of 1 ms and 600 scans were used for CP while a contact time of 0.5 ms and 250 scans were used for HETCOR.

^{1}H spin-lattice relaxation times T_1 were measured by either inversion recovery-cross polarization (IR-CP) or saturation recovery-cross polarization (SR-CP) techniques with a relaxation delay of 5 s and 432 scans for IR-CP and a relaxation delay of 1 s and 560 scans for SR-CP.

^{13}C spin-lattice relaxation times T_1 were measured by either IR or Torchia [41] techniques. IR was performed with a recycle delay of 1 s and 512 scans. Torchia experiments were performed with 600 scans, a contact time of 1 ms and a recycle delay of 2 s.

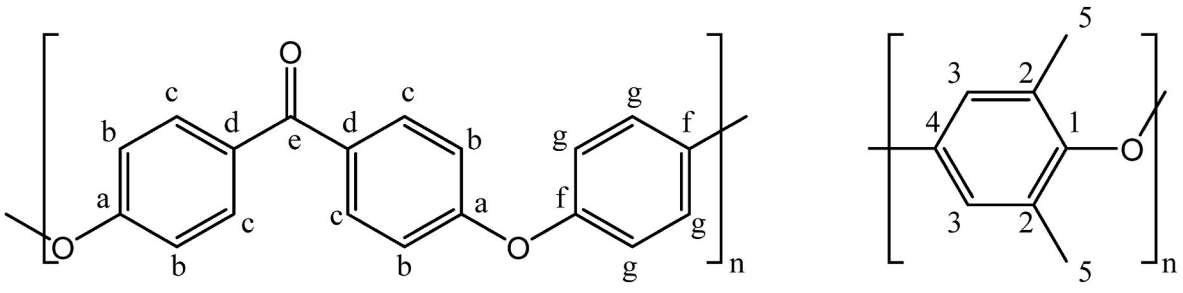

Fig. 1. Structures and positional labelling of PEEK (left) and PPO (right).

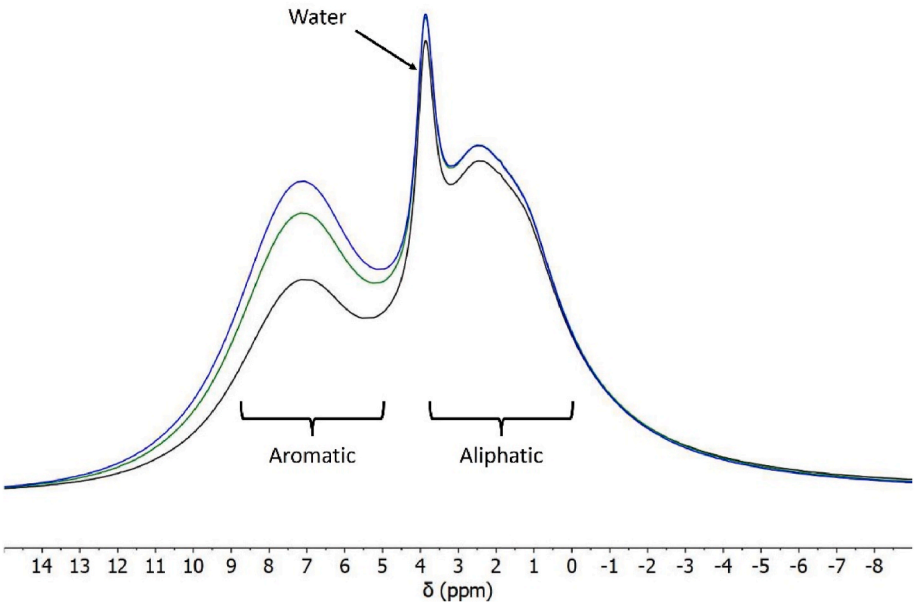

Fig. 2. Selection of ^{1}H MAS spectra of FAA-3-PK-130 recorded with different recycle delays: 1 s (black), 3 s (green), 15 s (blue). (For interpretation of the references to colour in this figure legend, the reader is referred to the Web version of this article.)

Differential Scanning Calorimetry (DSC) experiments were performed on a TA Instruments Discovery DSC 250 calorimeter. Aluminum Tzero pans closed with a Tzero hermetic lid were used and samples were analyzed in the range 30–180 °C with a cooling/heating rate of 10 °C/min. Thermograms are reported in exo-down visualization mode.

Scanning Electron Microscopy images were obtained using a FEI Quanta 450 FEG microscope. Samples have been metallised with gold before the analysis.

Micro-IR spectroscopy experiments were performed on a Thermo Fisher Nicolet iN10 IR-Microscope using a Germanium ATR crystal. Spectra were acquired using 64 scans with a resolution of the ATR tip of 10 μm × 10 μm.

3. Results & discussion

FAA-3-PK-130 is commercialized as a high performance anion exchange membrane with average thickness of 130 μm. This material is composed by two polymers, PEEK and PPO, whose structures are shown in Fig. 1. PPO is the ionomer in this system since it is endowed with a quaternary ammonium group, whose position and amount are not known [11,12].

3.1. Chemical structure of anion exchange sites

^{1}H MAS spectra were recorded on the membrane to preliminary

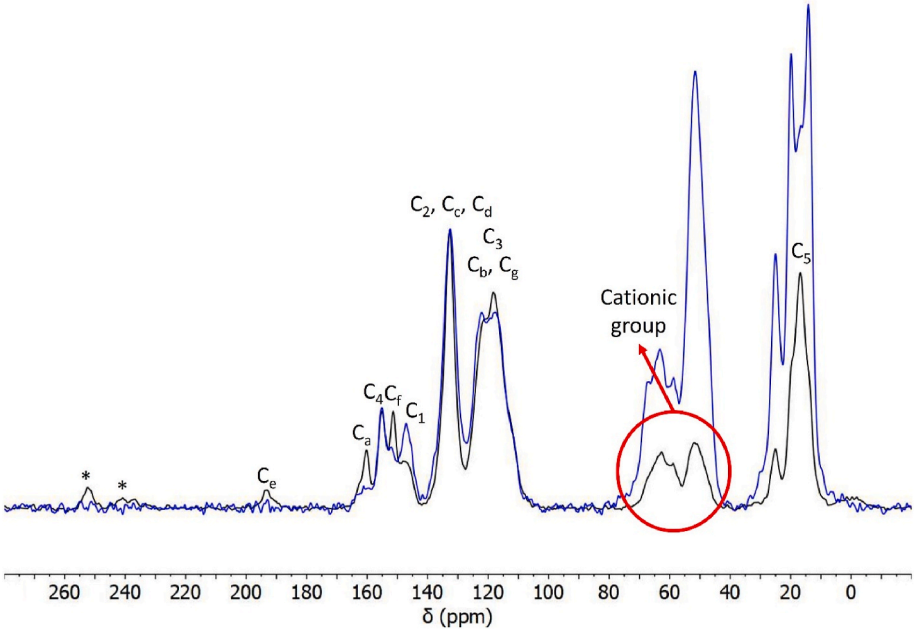

Fig. 3. ^{13}C CP MAS (black) and ^{13}C DE MAS (blue) spectra of FAA-3-PK-130 recorded at 15 kHz. The DE MAS spectrum was recorded with a recycle delay of 2 s. Carbons labelling refers to Fig. 1. Asterisks represent spinning sidebands. (For interpretation of the references to colour in this figure legend, the reader is referred to the Web version of this article.)

Table 1
Assignments of the peaks in the spectrum of Fig. 4 to the different PPO and PEEK carbons.

PPO		PEEK			
Nucleus	δ (ppm)	Nucleus	δ (ppm)	Nucleus	δ (ppm)
C_1	147.1	C_a	160.3	C_f	151.5
C_2	132.8	C_b	118.1	C_g	121.6
C_3	118.1	C_c	132.8		
C_4	155.1	C_d	132.8		
C_5	17.0	C_e	193.4		

study the material structure. The spectra were acquired using different recycle delays. Two different spectral regions could be identified. The first, centred around 2.4 ppm, is due to aliphatic protons, whereas the second, centred around 7.1 ppm, to aromatic protons. Moreover, the narrower signal at 3.9 ppm is due to the residual water in the membrane (Fig. 2).

Both PEEK and PPO contain aromatic protons and thus they contribute to the aromatic region, whereas the aliphatic one is addressed to PPO only. The two regions show different trends with the recycle delay, clearly indicating different ^{1}H spin-lattice relaxation times. As it will be better clarified later in this paper, this is due to an incomplete averaging action carried out by proton spin diffusion, and it suggests a phase separation between the two polymers on a ≈10–20 nm scale [42].

In a previous work on FAA-3, vibrational Raman results suggested the presence of CF_2 groups in the material [37], indicating that fluorinated sidechains are contained, as in Nafion [33]. To test this hypothesis, we acquired a ^{19}F MAS NMR spectrum of the membrane, which is reported in the Supplementary Material (Fig. S1): the spectrum of the membrane differs from that of background only for a quite narrow signal at −74.7 ppm, which can be assigned to hexafluoroisopropanol (HFIP) [43], typically used for the processing of polymers with low solubility in common organic solvents [44], which here should be somehow adsorbed on the membrane. Therefore, we can safely exclude the presence of fluorine in the structure of FAA-3-PK-130.

^{1}H–^{13}C CP MAS spectra (Fig. 3) were acquired using different contact times and MAS frequencies. This, together with the registration of 2D ^{1}H–^{13}C HETCOR spectra and the analysis of the ^{13}C SSNMR spectra of PPO [22] and PEEK [45] previously reported in the literature, allowed us to completely assign the ^{13}C isotropic peaks to the different carbons belonging to the two polymers (Table 1). According to the literature, the aliphatic region between 80 and 0 ppm should not contain any carbon signal arising from PPO and PEEK besides the peak of the methyl carbons of PPO, resonating at 17.0 ppm. However, a group of broad signals between 70 and 45 ppm, as well as a narrow signal at 25.2 ppm, are also clearly present in the spectra of the investigated membrane. Considering the chemical shift values and the broadness of the signals, the first group of signals could be ascribed to aliphatic carbons bound to a nitrogen atom. Their unusual and broad shape arises from the residual ^{13}C–^{14}N dipolar coupling [46,47]. The narrow peak at 25.2 ppm, instead, can be tentatively ascribed to a methyl carbon bound to an aliphatic group. From now on, we will refer to the 70-20 ppm region as the "functionalization region" containing the resonances from the anion exchange sites.

A ^{13}C DE-MAS spectrum was recorded with a short relaxation delay of 2 s in order to identify carbons with short spin-lattice relaxation times and, correspondingly, sites characterised by high mobility (Fig. 4). Notably, in this spectrum the functionalization region showed a considerable relative intensity enhancement, if compared to all the other signals, with respect to the CP-MAS spectrum (Fig. 4). By recording DE-MAS ^{13}C spectra at different relaxation delays, it was seen that a relaxation delay of 40 s was sufficient to achieve complete relaxation of the region 0–80 ppm (Fig. S2), including the methyl carbons of PPO and the whole functionalization region, thus enabling a quantitative analysis of the peak integrals of this spectral region. On the contrary, the aromatic carbons did not completely relax even using 300 s as relaxation delay. This behaviour is not unexpected since both PEEK [48] and PPO [49] are glassy polymers at room temperature with macromolecular local motions almost frozen, with the reasonable exception of the reorientation of side-chain methyl groups. These observations clearly indicate that the carbons belonging to the functionalization group(s) experience the shortest ^{13}C spin-lattice relaxation times.

Table 2
^{13}C spin-lattice relaxation times measured at different temperatures for the carbons of the functionalization group.

T (K)	$C_{1'}$ (62.8 ppm)		$C_{2'}$ (51.6 ppm)	$C_{3'}$ (25.2 ppm)
	$T_{1,s}$ (s)	$T_{1,l}$ (s)	T_1 (s)	T_1 (s)
248	0.76	6.0	0.12	0.43
253			0.12	0.47
263	0.76	6.2	0.12	0.52
273	0.71	5.1	0.13	0.52
283	0.59	6.0	0.12	0.55
298	0.51	5.5	0.13	0.60
303			0.14	0.63
308	0.55	5.5		
313	0.60	4.8	0.15	0.60
323			0.16	0.70
333			0.18	0.64
343	0.57	4.3	0.18	0.74

The ^{13}C DE spectrum obtained with a relaxation delay of 40 s was used to deconvolute the regions of the functionalization and of the PPO methyl carbons (Fig. 4).

The region between 80 ppm and 40 ppm could be fit with two signals (1′ and 2′) with a similar integral and thus they should correspond to two distinct carbon sites present in the same amount. On the other hand, the sharp signal at 25.2 ppm (3′) is characterized by about half the integral of 1′ and 2′. This indicates that the number of carbons 3′ is half that of either carbons 1′ or 2′.

The most intense peak at about 17 ppm can be deconvoluted using a combination of three different signals centred at 20.0 ppm (4′), 17.0 ppm (5) and 14.2 ppm (6′). We can safely assign 4′ and 6′ to the functionalization moiety since in the spectrum of neat PPO only the central signal 5, belonging to the two methyl groups, is observed [22,50]. It should be noted that 4′ and 6′ have the same integral (within the experimental error) of 3′, indicating that each of these carbons is present in the same amount of 3'.

To further identify the nature of the functionalization group, ^{13}C spin-lattice relaxation times were measured using the Torchia pulse sequence [41] at different temperatures and the results are reported in Table 2. A biexponential relaxation decay was found for carbon 1′ at all temperatures with a relative weight of 50 % for each exponential. On the other hand, carbons 2′ and 3′ show a mono-exponential decay, with a much shorter relaxation time that indeed required the use of the inversion recovery pulse sequence to obtain a more precise measurement of the corresponding spin lattice relaxation times.

By looking at the trend of T_1 *vs* temperature, it is possible to see that T_1 is increasing with increasing temperature for carbons 2′ and 3′, indicating that spin lattice relaxation of these nuclei is driven by motions that are fast with respect to the carbon ^{13}C Larmor frequency ($\omega_0\tau_c < 1$, where τ_c is the correlation time of the motion and $\omega_0/2\pi \approx 125$ MHz). In the case of carbon 2′, T_1 approaches a minimum at low temperature, corresponding to the condition $\omega_0\tau_c \approx 1$. The trend is more complex, due to the biexponential relaxation, and less pronounced for carbon 1′. In order to better visualize and analyse these trends, relaxation times have been reported in Fig. 5 in Arrhenius-type plots (ln ($1/T_1$) *vs* 1000/T). Here, a linear trend is expected when the motion is very fast with respect to the carbon Larmor frequency ($\omega_0\tau_c \ll 1$). This condition is always met for carbon 3' and above 283 K for carbon 2′. In these cases, it is possible to easily fit the data to determine the activation energy of the motions affecting the relaxation. The activation energies resulted about 5.6 and

Peak	δ (ppm)	Integral
1′	62.8	100
2′	51.6	94
3′	25.2	55
4′	20.0	58
5	17.0	153
6′	14.2	46

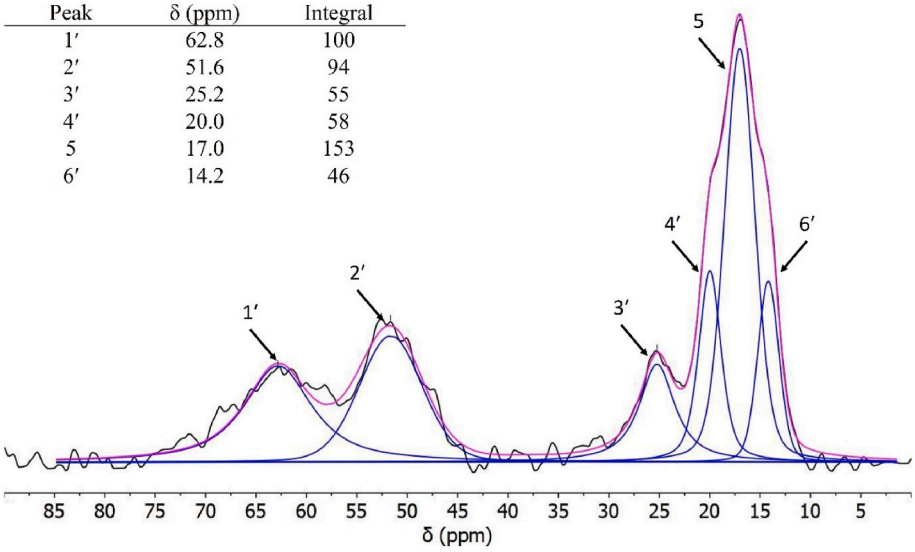

Fig. 4. Expansion of the aliphatic and functionalization region of the ^{13}C DE MAS spectrum of FAA-3-PK-130 recorded with a recycle delay of 40 s (black) and corresponding deconvolution (violet): the individual peaks found by the deconvolution are reported in blue. (For interpretation of the references to colour in this figure legend, the reader is referred to the Web version of this article.)

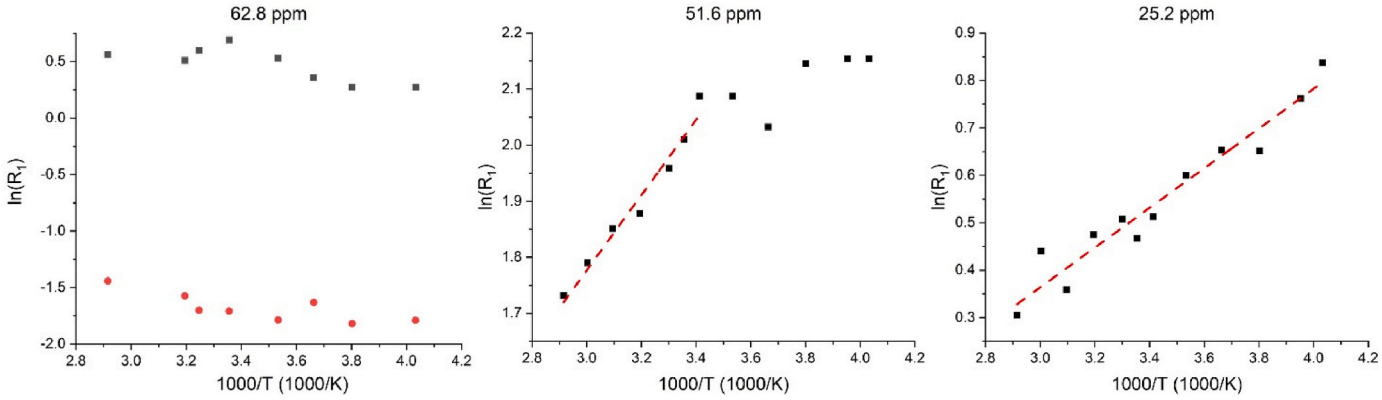

Fig. 5. Plot of ^{13}C ln $(1/T_1)$ as a function of the inverse of temperature. Linear fits for T_1 in fast motion regimes are reported.

3.5 kJ/mol for carbons 2′ and 3′, respectively. These two values are compatible with the rotational barrier of a methyl group, which usually ranges from 4 kJ/mol to 20 kJ/mol [51]. Carbon 2′, which should belong to a methyl group bound to a nitrogen atom, shows an activation energy even smaller than that expected for a $^{+}N–CH_3$ rotational barrier in crystalline ammonium salts [52]. However, a small activation energy for the rotation of a methyl bound to nitrogen has been previously reported and it is consistent with the value obtained for carbon 2′ [53].

On the basis of the carbons ratio 1':2':3':4':6' ≈ 2:2:1:1:1, considering that carbons 1′ and 2′ seem directly bonded to nitrogen atoms and that 2′ should belong to methyl carbons, we can hypothesize for the functionalization group the structure $–[RNR'(CH_3)_2]^{+}$, with R≠R′, and R somehow bonded to PPO. Further information could be extracted from $^{1}H–^{13}C$ HETCOR spectra (Fig. S3). In fact, the ^{1}H signal at 3.5 ppm, correlating with the ^{13}C signals at 58.8 ppm (ascribed to carbons directly bound to nitrogen), also shows a correlation peak with the ^{13}C signal at 25.2 ppm, attributed to a methyl carbon. These correlations are representative of an ethyl group bound to the nitrogen atom (R' = CH_2CH_3).

The fourth alkyl group (R) can be identified with a CH_2 group, connecting the nitrogen atom of the quaternary ammonium group to the phenyl ring of PPO after a benzylic substitution. This type of functionalization is common in PPO-based ionomers since it can be easily achieved through halo-methylation [54,55] or radical halogenation [9, 54–57]. The combination of all previous observations brings to the structure of the ammonium group reported in Fig. 6, also reporting the assignment of the ^{13}C signals. This is also supported by the presence of the two signals 4′ and 6′, that can be ascribed to the two methyl carbons of the phenyl ring of PPO made inequivalent by the occurrence of the functionalization on the same ring, which removes the symmetry respect to its para axis. The integral ratios 4':5:6' ≈ 1:3:1 in the quantitative carbon spectrum (Fig. 4) can be used to derive a degree of functionalization of about 40 % by mol for PPO in FAA-3-PK-130.

3.2. Phase properties

Since two different polymers constitute this material, it is important to determine the degree of mixing/separation of their phase domains. This aspect has been investigated by using ^{1}H spin lattice relaxation times T_1, since for abundant nuclei they are affected by spin diffusion that tends to average out ^{1}H longitudinal magnetization gradients in solids. As a result, for homogeneous materials on the nanometer scale, a single ^{1}H T_1 is usually observed. Instead, as anticipated before, a different result is obtained when a heterophasic material presents phase domains with average dimensions larger than 10–20 nm. In this case, two or more distinct proton T_1's are observed because the diffusion of magnetization is not able to efficiently average out the magnetization

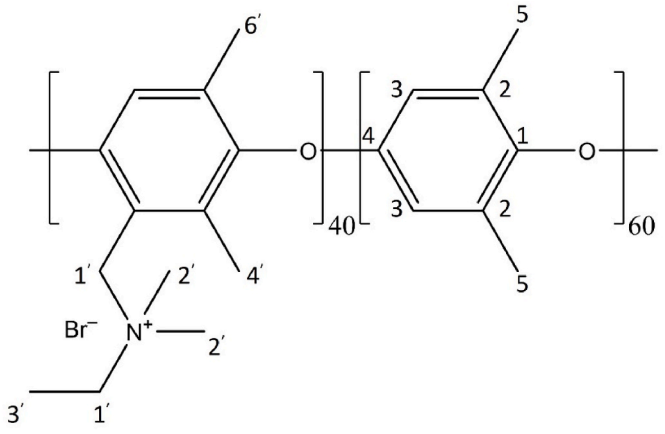

Fig. 6. Proposed structure of the ionomer.

gradient on the timescale of the relaxation process. This property allows the exploration of phase separation and domain dimension on the nanometric scale through the measurement of proton spin-lattice relaxation times [18,42]. In this work, proton T_1 has been measured through either IR-CP or SR-CP pulse sequences. When using these sequences, proton spin lattice relaxation times can be obtained from the integrals of different carbon signals as a function of the relevant variable delay. Each carbon signal reveals the relaxation times of the neighbouring protons, so distinct carbon signals can be used to measure the ^{1}H T_1's of different phases, exploiting the better spectral resolution of ^{13}C spectra.

Two different ^{1}H T_1's of about 2.45 and 0.41 s were measured (Fig. 7). The longest comes from the ^{13}C peak at 193.4 ppm, assigned to the ketone group of PEEK; the shortest is instead measured from the ^{13}C peaks at about 20 ppm, mainly arising from the methyl groups of PPO. Interestingly, the aromatic ^{13}C signals, arising from both PPO and PEEK, show a biexponential relaxation behaviour, given by the combination of the long and short ^{1}H T_1 components ascribed to PEEK and PPO protons, respectively. The fact that PPO and PEEK show two clearly distinct proton spin lattice relaxation times indicates that they are well phase-separated on the 10–20 nm spatial scale, i.e. the dimensions of their average phase domains are much larger than 20 nm.

Further information can be extracted if the region of the quaternary ammonium group is considered. In fact, from the ^{13}C signals at about 60 ppm, due to the functionalizing group, a ^{1}H T_1 of 0.42 s, coincident with that of the protons of PPO, is obtained. This undoubtedly indicates that the functionalization with the quaternary ammonium moiety takes place only on PPO, possibly because PEEK is included in a second step of the preparation of the material.

To identify the nature of FAA-3-PK-130, a micro-ATR analysis was also performed (Fig. S5). The sample resulted made of a mesh of polymeric fibres: the IR spectrum of PPO was always obtained [58], while the presence of PEEK was only visible by focusing the ATR tip on some parts of the sample, when the characteristic C═O stretching [59] at 1653 cm^{-1} was observed. Micro-ATR was also performed on the cross-section of the material (Fig. S6). In this case, the spectra of either PPO [58] or PEEK [59] were obtained on different spots of the section. This observation points towards the hypothesis that both polymers are included in the observed fibres, but that they are phase separated on the micrometric scale in agreement with SSNMR results.

Finally, DSC analysis was carried out to investigate the phase properties of the two polymers in FAA-3-PK-130. A small temperature range (20–180 °C) could be explored due to the thermal decomposition of the ionomer above 200 °C (Fig. S8). In this temperature range, the glass transition of PEEK (about 145 °C) and crystallisation of PEEK (around 175 °C) were expected [60], but they could not be observed (Fig. S8). This result suggests a high crystallinity of PEEK in the material. However, this hypothesis could not be verified by ^{13}C SSNMR spectra

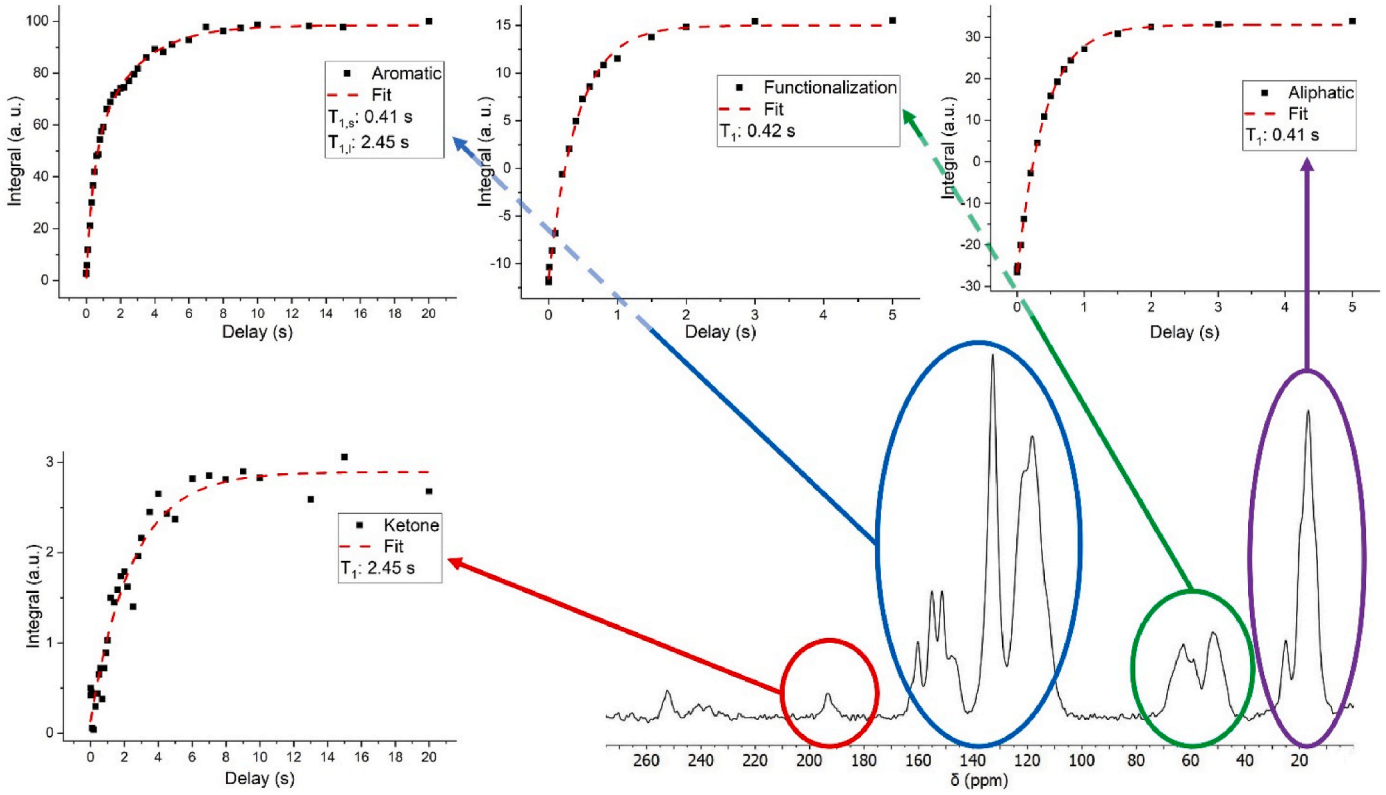

Fig. 7. ^{1}H spin lattice relaxation times obtained through techniques exploiting cross polarization from ^{1}H to ^{13}C. SR-CP has been used for the ketone and for the aromatic signals. IR-CP has been used for the functionalization and for the aliphatic region of PPO.

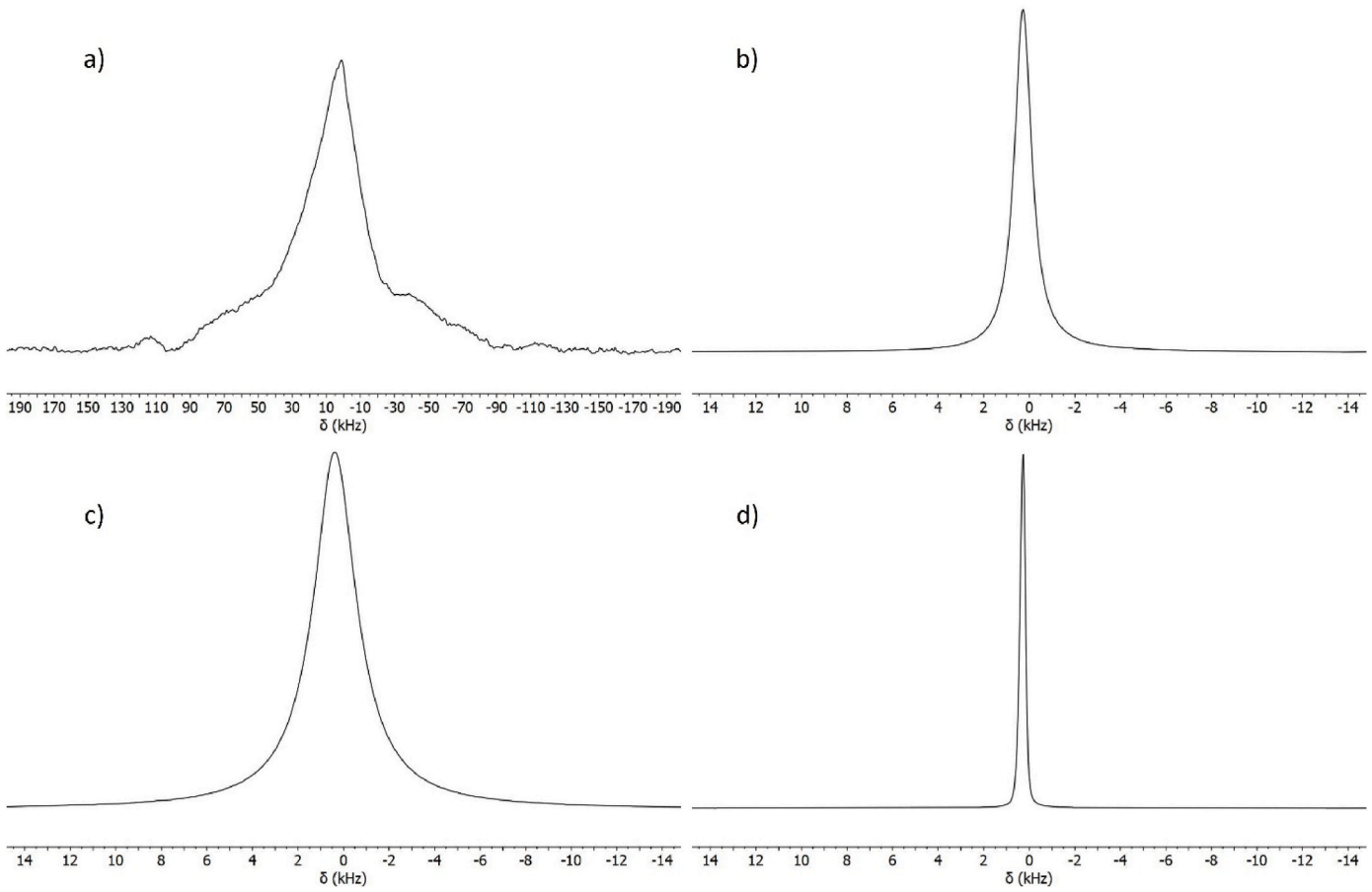

Fig. 8. Static ^{2}H NMR spectra of Fumasep FAA-3-PK-130 after hydration with D_2O under a controlled relative humidity of ≈6 % (a and b) or ≈ 84 % (c and d). Spectra a and c have been recorded at 243 K while spectra c and d at 343 K. Spectra are not on the same scale.

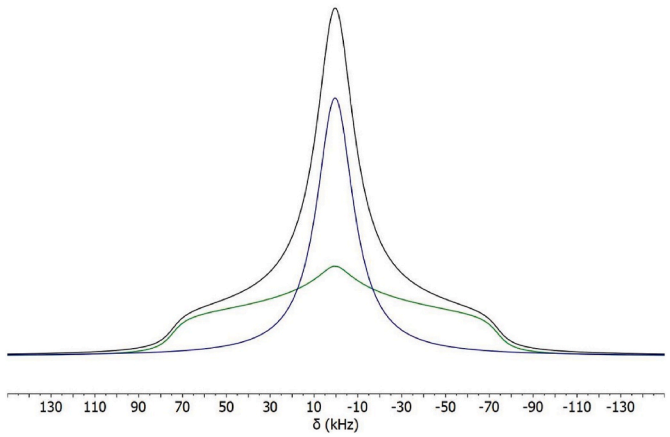

Fig. 9. Simulation of the ^{2}H static pattern recorded at 243 K for Fumasep FAA-3-PK-130 after hydration under a controlled relative humidity of ≈6 %. The sum of two different lineshapes was used. The Lorentzian peak (blue) represents water that is free to rotate in the ionic channels. The wider pattern (green) represents motionally restricted water that undergoes C_2-jumps on a fast timescale. The sum of the two patterns is reported in black. (For interpretation of the references to colour in this figure legend, the reader is referred to the Web version of this article.)

because crystalline and amorphous PEEK mainly differ in the region between 100 and 140 ppm [45], where PEEK signals are strongly superimposed to those of PPO. Moreover, no information on the crystallinity of PPO could be obtained by either DSC or ^{13}C SSNMR. Indeed, the glass transition of pure PPO takes place at 215 °C [49] that is around the decomposition temperature of the material. Moreover, ^{13}C SSNMR spectra of semicrystalline and amorphous PPO do not show significant differences [22,61].

3.3. Water-ions interactions in ionic channels

Static ^{2}H NMR spectra have been recorded on Fumasep FAA-3-PK-130 at different temperatures after hydration with deuterated water under controlled relative humidity (RH) (Fig. 8).

The sample hydrated over a saturated solution of LiBr (RH ≈ 6 %) shows a complex static spectral pattern when cooled down to 243 K (Fig. 8a). This pattern contains a broad central peak with a width of approximately 35 kHz with two shoulders approximately 100 kHz apart. Even if the temperature is below zero, the typical powder pattern of ice cannot be identified [62]. The ^{2}H static spectrum could be simulated using a combination of two static quadrupolar patterns, as reported in Fig. 9. The Lorentzian peak is characterized by a null quadrupolar constant C_Q and represents water in an isotropic environment, subjected to both molecular diffusion and rotation. However, the linewidth is larger than that expected for bulk water, probably due to the partially restricted environment of ionic channels. The second contribution to the ^{2}H spectrum is characterized by a quadrupolar constant C_Q = 99 kHz and an asymmetry parameter $\eta = 1$. This pattern can be obtained when water molecules do not freely reorient, but they experience fast two-site jumping around the C_2 symmetry axis of water [63,64]. The interpretation of the lineshape is far from trivial, but a first hypothesis can be formulated from Gierke's model of hydration of IEMs [65]. In fact, when a small amount of water is adsorbed, small clusters containing ions and

water are formed. In these clusters water strongly interacts with ions, resulting in impaired mobility. The composition of the ^{2}H lineshape suggests that at least two types of water-ions clusters are formed. These clusters mainly differ by the presence or not of free water inside the cluster itself. Free water can diffuse and rotate and exchanges with water bound to ions, giving the Lorentzian lineshape (type-I clusters). However, if free water is not present, water remains bound to ions and the only fast motion that can experience is the C_2-jumping, resulting in the broader lineshape (type-II clusters). The ratio of the integrals of these two spectral lineshape components is 53:47, representative of the percentage of water molecules in type-II and type-I clusters, respectively.

Upon heating at 343 K (Fig. 8b), the lineshape of deuterium deeply changes and only one peak with a width of about 1 kHz is observed due to the mobilization of the water in type-II clusters.

Different results are obtained for the sample hydrated over a saturated solution of KCl (RH ≈ 84 %). In fact, even at 243 K (Fig. 8c) the lineshape appears quite narrow (about 2.4 kHz) and becomes much narrower at 343 K (Fig. 8d) (280 Hz). This suggests that all the water molecules belong to the same wide ionic channels, where water can differently interact with ions depending on their distance from them. However, the presence of a single spectral lineshape indicates that water molecules far from ions can exchange with those that are near the walls of the ionic channels, in the so called ion depletion layer [65]. Water is almost liquid-like: even at 243 K, although experiencing a sensibly reduced mobility, it does not freeze, confirming that it is not adsorbed on the surface of the material, but rather confined inside the ionic channels.

4. Conclusions

Fumasep FAA-3-PK-130 is a commercially available and benchmark AEM based on a blend of PPO and PEEK, but many of its structural features are almost unknown. A multinuclear SSNMR approach was effectively used to unravel the structure, position, and amount of the functionalizing ammonium group, which are very important aspects to understand the molecular origin of the macroscopic behaviour of this material, but which were not known so far. Notably, by combining ^{1}H, ^{19}F, ^{13}C MAS spectra, ^{1}H–^{13}C HETCOR 2D spectra, as well as ^{13}C spin-lattice relaxation times, it was found that the anion exchange sites consist of methylene-dimethyl-ethyl ammonium units bonded to PPO phenyl group on one of the two arylic positions, possibly via a halomethylation process, and with a degree of functionalization of about 40 %.

^{1}H spin-lattice relaxation times were measured exploiting the better spectral resolution of ^{13}C nuclei, thus allowing the detection of a phase separation between PEEK and PPO on a 10–20 nm spatial scale. This was confirmed by a Micro-ATR analysis, which established that phase separation should occur on the even larger micrometric scale.

From ^{2}H static spectra it was possible to investigate the presence and nature of ionic channels in samples prepared by hydration with deuterated water in a controlled environment. No freezing of water was observed upon cooling down to 243 K, indicating the confinement of water molecules within pores of either nanometric or sub-nanometric dimensions. At low hydration levels, two types of water-ion clusters were detected, one of which containing, at 243 K, only water molecules with their tumbling motion hampered by their strong interaction with ions. On the other hand, at higher hydration levels, all the ion channels contain fast-exchanging interacting and non-interacting water molecules.

In conclusion, multinuclear SSNMR approach was found to be useful to disclose structural and dynamic features of FAA-3-PK-130. This information can be precious to understand the molecular origin of the macroscopic properties of the membrane and can be exploited to devise systems with similar performances.

CRediT authorship contribution statement

Andrea Giovanelli: Writing – review & editing, Writing – original draft, Visualization, Validation, Methodology, Investigation, Formal analysis, Data curation, Conceptualization. **Alfonso Pozio:** Validation, Resources, Project administration, Funding acquisition, Conceptualization. **Andrea Pucci:** Writing – review & editing, Writing – original draft, Validation, Supervision, Resources, Project administration, Methodology, Investigation, Funding acquisition, Data curation, Conceptualization. **Marco Geppi:** Writing – review & editing, Writing – original draft, Validation, Supervision, Resources, Project administration, Methodology, Investigation, Funding acquisition, Data curation, Conceptualization. **Francesca Martini:** Writing – review & editing, Validation, Supervision, Resources, Project administration, Funding acquisition, Conceptualization.

Declaration of competing interest

The authors declare that they have no known competing financial interests or personal relationships that could have appeared to influence the work reported in this paper.

Data availability

Data will be made available on request.

Acknowledgements

This research was partially funded by European Union, NextGenerationEU PRIN-PNRR 2022 In-MoTion, the University of Pisa grant PRA_2022_34 “Optimizing intermolecular interactions for recognition catalysis and green chemistry” and by ENEA (Ente per le Nuove tecnologie, l’Energia e l’Ambiente). Elia Rossi is acknowledged for his help in performing SSNMR measurements. Dr. Marco Carlotti is acknowledged for his help in designing the graphical abstract.

CISUP (Center for Instrument Sharing-University of Pisa) is acknowledged for the use of the Bruker Avance Neo 500 solid-state NMR spectrometer.

Appendix A. Supplementary data

Supplementary data to this article can be found online at https://doi.org/10.1016/j.polymer.2024.127536.

References

[1] D. Hua, J. Huang, E. Fabbri, M. Rafique, B. Song, Development of anion exchange membrane water electrolysis and the associated challenges: a review, Chemelectrochem 10 (2023) e202200999, https://doi.org/10.1002/celc.202200999.

[2] N. Du, C. Roy, R. Peach, M. Turnbull, S. Thiele, C. Bock, Anion-exchange membrane water electrolyzers, Chem. Rev. 122 (2022) 11830–11895, https://doi.org/10.1021/acs.chemrev.1c00854.

[3] P. Zuo, Z. Xu, Q. Zhu, J. Ran, L. Ge, X. Ge, L. Wu, Z. Yang, T. Xu, Ion exchange membranes: constructing and tuning ion transport channels, Adv. Funct. Mater. 32 (2022) 2207366, https://doi.org/10.1002/adfm.202207366.

[4] M.G. Marino, K.D. Kreuer, Alkaline stability of quaternary ammonium cations for alkaline fuel cell membranes and ionic liquids, ChemSusChem 8 (2015) 513–523, https://doi.org/10.1002/cssc.201403022.

[5] O. Racchi, R. Baldassari, E. Araya-Hermosilla, V. Mattoli, P. Minei, A. Pozio, A. Pucci, Polyketone-based anion-exchange membranes for alkaline water electrolysis, Polymers 15 (2023) 2027, https://doi.org/10.3390/polym15092027.

[6] X. Yan, G. He, X. Wu, J. Benziger, Ion and water transport in functionalized PEEK membranes, J. Membr. Sci. 429 (2013) 13–22, https://doi.org/10.1016/j.memsci.2012.11.026.

[7] J. Qian, C. Wang, X. Zhang, J. Hu, X. Zhao, J. Li, Q. Ren, Quaternary ammonium-functionalized crosslinked poly(aryl ether sulfone)s anion exchange membranes with enhanced alkaline stability for water electrolysis, J. Membr. Sci. 685 (2023) 121946, https://doi.org/10.1016/j.memsci.2023.121946.

[8] M. Hu, L. Ding, M.A. Shehzad, Q. Ge, Y. Liu, Z. Yang, L. Wu, T. Xu, Comb-shaped anion exchange membrane with densely grafted short chains or loosely grafted

long chains? J. Membr. Sci. 585 (2019) 150–156, https://doi.org/10.1016/j.memsci.2019.05.034.
[9] J. Han, S. Gong, Z. Peng, X. Cheng, Y. Li, H. Peng, Y. Zhu, Z. Ren, L. Xiao, L. Zhuang, Comb-shaped anion exchange membranes: hydrophobic side chains grafted onto backbones or linked to cations? J. Membr. Sci. 626 (2021) 119096 https://doi.org/10.1016/j.memsci.2021.119096.
[10] G.H.A. Wijaya, K.S. Im, S.Y. Nam, Advancements in commercial anion exchange membranes: a review of membrane properties in water electrolysis applications, Desalination Water Treat. 320 (2024) 100605, https://doi.org/10.1016/j.dwt.2024.100605.
[11] D. Henkensmeier, M. Najibah, C. Harms, J. Žitka, J. Hnát, K. Bouzek, Overview: state-of-the art commercial membranes for anion exchange membrane water electrolysis, J. Electrochem. Energy Convers. Storage 18 (2021) 024001, https://doi.org/10.1115/1.4047963.
[12] Technical Data Sheet - Fumasep FAA-3-PK-130, Fumatech GmbH, (n.d).
[13] N.U. Saidin, O.S. Jehan, K.S. Leong, T.F. Choo, W.Y. Wong, K.S. Loh, R.M. Yunus, Influence of ionomer concentration and membrane thickness on membrane electrode assembly in alkaline fuel cell performance, Asia Pac. J. Chem. Eng. 19 (2024) e3024, https://doi.org/10.1002/apj.3024.
[14] H. Tang, Y. Liao, L. Wang, Review of the state-of-the-art anion exchange membranes, in: Green Hydrog. Prod. Water Electrolysis, CRC Press, 2024.
[15] I. Arunkumar, R. Gokulapriyan, V. Sakthivel, A.R. Kim, M.S. Oh, J.Y. Lee, S. Kim, S. Lee, D.J. Yoo, Functionalized graphene nanofiber-incorporated fumion anion-exchange membranes with enhanced alkaline stability and fuel-cell performances, ACS Appl. Energy Mater. 6 (2023) 7702–7713, https://doi.org/10.1021/acsaem.3c01182.
[16] S. Rakhshani, R. Araneo, A. Pucci, A. Rinaldi, C. Giuliani, A. Pozio, Synthesis and characterization of a composite anion exchange membrane for water electrolyzers (AEMWE), Membranes 13 (2023) 109, https://doi.org/10.3390/membranes13010109.
[17] S. Favero, I.E.L. Stephens, M.-M. Titirci, Anion exchange ionomers: design considerations and recent advances - an electrochemical perspective, Adv. Mater. 36 (2024) 2308238, https://doi.org/10.1002/adma.202308238.
[18] K. Müller, M. Geppi, Solid State NMR: Principles, Methods, and Applications, Wiley & Sons Inc., 2021.
[19] I. Ando, T. Yamanobe, S. Akiyama, T. Komoto, H. Sato, T. Fujito, K. Deguchi, M. Imanari, Polyethylene structure in the solid state as studied by variable-temperature 13C CP/MAS n.m.r. spectroscopy, Solid State Commun. 62 (1987) 785–788, https://doi.org/10.1016/0038-1098(87)90049-4.
[20] A. Asano, K. Takegoshi, K. Hikichi, Solid-state NMR study of miscibility and phase-separation of polymer blend: polycarbonate/poly(methyl methacrylate), Polym. J. 24 (1992) 555–562, https://doi.org/10.1016/0032-3861(93)90873-9.
[21] M. Faraj, M. Boccia, H. Miller, F. Martini, S. Borsacchi, M. Geppi, A. Pucci, New LDPE based anion-exchange membranes for alkaline solid polymeric electrolyte water electrolysis, Int. J. Hydrogen Energy 37 (2012) 14992–15002, https://doi.org/10.1016/j.ijhydene.2012.08.012.
[22] A. Bielecki, D.P. Burum, D.M. Rice, F.E. Karasz, Solid-state two-dimensional carbon-13-proton correlation (HETCOR) NMR spectrum of amorphous poly(2,6-dimethyl-p-phenylene oxide) (PPO), Macromolecules 24 (1991) 4820–4822, https://doi.org/10.1021/ma00017a014.
[23] M. Becher, S. Becker, L. Hecht, M. Vogel, From local to diffusive dynamics in polymer electrolytes: NMR studies on coupling of polymer and ion dynamics across length and time scales, Macromolecules 52 (2019) 9128–9139, https://doi.org/10.1021/acs.macromol.9b01400.
[24] G. Mollica, C. Forte, M. Malvaldi, M. Geppi, Dynamics of Ethylene−Propylene random copolymers by 1H and 13C solid-state NMR, J. Phys. Chem. B 115 (2011) 1978–1985, https://doi.org/10.1021/jp111435s.
[25] L. Calucci, S. Pizzanelli, A. Mandoli, A. Birczyński, Z.T. Lalowicz, C. De Monte, L. Ricci, S. Bronco, Unravelling main- and side-chain motions in polymers with NMR spectroscopy and relaxometry: the case of polyvinyl butyral, Polymers 13 (2021) 2686, https://doi.org/10.3390/polym13162686.
[26] F. Martini, S. Borsacchi, S. Spera, C. Carbonera, A. Cominetti, M. Geppi, P3HT/PCBM photoactive materials for solar cells: morphology and dynamics by means of solid-state NMR, J. Phys. Chem. C 117 (2013) 131–139, https://doi.org/10.1021/jp3103904.
[27] P. Mustarelli, E. Quartarone, C. Capiglia, C. Tomasi, P. Ferloni, A. Magistris, Host–guest interactions in fluorinated polymer electrolytes: a 7Li-13C NMR study, J. Chem. Phys. 111 (1999) 3761–3768, https://doi.org/10.1063/1.479656.
[28] P. Pal, A. Ghosh, Ion transport and segmental dynamics in cross-linked poly (ethylene glycol) diacrylate-based solid-like polymer electrolytes, J. Phys. Chem. C 126 (2022) 4799–4806, https://doi.org/10.1021/acs.jpcc.1c10456.
[29] G. Ye, C.A. Hayden, G.R. Goward, Proton dynamics of nafion and nafion/SiO2 composites by solid state NMR and pulse field gradient NMR, Macromolecules 40 (2007) 1529–1537, https://doi.org/10.1021/ma0621876.
[30] V.I. Volkov, A.V. Chernyak, O.I. Gnezdilov, V.D. Skirda, Hydration, self-diffusion and ionic conductivity of Li+, Na+ and Cs+ cations in Nafion membrane studied by NMR, Solid State Ionics 364 (2021) 115627, https://doi.org/10.1016/j.ssi.2021.115627.
[31] M.G. Marino, J.P. Melchior, A. Wohlfarth, K.D. Kreuer, Hydroxide, halide and water transport in a model anion exchange membrane, J. Membr. Sci. 464 (2014) 61–71, https://doi.org/10.1016/j.memsci.2014.04.003.
[32] X. Kong, K. Wadhwa, J.G. Verkade, K. Schmidt-Rohr, Determination of the structure of a novel anion exchange fuel cell membrane by solid-state nuclear magnetic resonance spectroscopy, Macromolecules 42 (2009) 1659–1664, https://doi.org/10.1021/ma802613k.
[33] K.A. Mauritz, R.B. Moore, State of understanding of nafion, Chem. Rev. 104 (2004) 4535–4586, https://doi.org/10.1021/cr0207123.
[34] H.-G. Haubold, Th Vad, H. Jungbluth, P. Hiller, Nano structure of NAFION: a SAXS study, Electrochim. Acta 46 (2001) 1559–1563, https://doi.org/10.1016/S0013-4686(00)00753-2.
[35] G. Gebel, O. Diat, Neutron and X-ray scattering: suitable tools for studying ionomer membranes, Fuel Cell. 5 (2005) 261–276, https://doi.org/10.1002/fuce.200400080.
[36] A.M. Barnes, B. Liu, S.K. Buratto, Humidity-dependent surface structure and hydroxide conductance of a model quaternary ammonium anion exchange membrane, Langmuir 35 (2019), https://doi.org/10.1021/acs.langmuir.9b02160.
[37] G. Chikvaidze, J. Gabrusenoks, J. Kleperis, G. Vaivars, Application of micro Raman spectroscopy to industrial FC membranes, J. Phys. Conf. Ser. 93 (2007) 012026, https://doi.org/10.1088/1742-6596/93/1/012026.
[38] L. Greenspan, Humidity fixed points of binary saturated aqueous solutions, J. Res. Natl. Bur. Stand. Sect. Phys. Chem. 81A (1977) 89, https://doi.org/10.6028/jres.081A.011.
[39] R.K. Harris, E.D. Becker, S.M. Cabral de Menezes, R. Goodfellow, P. Granger, NMR nomenclature: nuclear spin properties and conventions for chemical shifts: IUPAC recommendations 2001, Solid State Nucl. Magn. Reson. 22 (2002) 458–483, https://doi.org/10.1002/cmr.10035.
[40] B.M. Fung, A.K. Khitrin, K. Ermolaev, An improved broadband decoupling sequence for liquid crystals and solids, J. Magn. Reson. 142 (2000) 97–101, https://doi.org/10.1006/jmre.1999.1896.
[41] D.A. Torchia, The measurement of proton-enhanced carbon-13 T1 values by a method which suppresses artifacts, J. Magn. Reson. 30 (1978) 613–616, https://doi.org/10.1016/0022-2364(78)90288-3, 1969.
[42] J. Clauss, K. Schmidt-Rohr, H.W. Spiess, Determination of domain sizes in heterogeneous polymers by solid-state NMR, Acta Polym. 44 (1993) 1–17, https://doi.org/10.1002/actp.1993.010440101.
[43] T. Hayasaka, Y. Katsuhara, T. Kume, T. Yamazaki, HF-mediated equilibrium between fluorinated ketones and the corresponding α-fluoroalcohols, Tetrahedron 67 (2011) 2215–2219, https://doi.org/10.1016/j.tet.2011.01.087.
[44] H. Xia, Y. Hashimoto, T. Morita, T. Hirai, Formation of polyketone particle structure by hexafluoroisopropanol solvent evaporation and effects of plasticizer addition, J. Polym. Sci., Part B: Polym. Phys. 52 (2014) 887–892, https://doi.org/10.1002/polb.23501.
[45] M.D. Poliks, J. Schaefer, Characterization of the chain dynamics of PEEK by CPMAS carbon-13 NMR, Macromolecules 23 (1990) 3426–3431, https://doi.org/10.1021/ma00216a007.
[46] C.J. Groombridge, R.K. Harris, K.J. Packer, B.J. Say, S.F. Tanner, High-resolution 13C n.m.r. spectra of solid nitrogen-containing compounds, J. Chem. Soc. Chem. Commun. (1980) 174–175, https://doi.org/10.1039/C39800000174.
[47] J.G. Hexem, M.H. Frey, S.J. Opella, Molecular and structural information from 14N–13C dipolar couplings manifested in high resolution 13C NMR spectra of solids, J. Chem. Phys. 77 (1982) 3847–3856, https://doi.org/10.1063/1.444338.
[48] M. Doumeng, L. Makhlouf, F. Berthet, O. Marsan, K. Delbé, J. Denape, F. Chabert, A comparative study of the crystallinity of polyetheretherketone by using density, DSC, XRD, and Raman spectroscopy techniques, Polym. Test. 93 (2021) 106878, https://doi.org/10.1016/j.polymertesting.2020.106878.
[49] H.-S. Dang, E.A. Weiber, P. Jannasch, Poly(phenylene oxide) functionalized with quaternary ammonium groups via flexible alkyl spacers for high-performance anion exchange membranes, J. Mater. Chem. A 3 (2015) 5280–5284, https://doi.org/10.1039/C5TA00350D.
[50] E.M. Woo, I.-C. Chou, L.L. Chang, H.-M. Kao, Solid-state NMR characterization on the molecular-level homogeneity in lower critical solution temparature mixtures of poly(α-methyl styrene) and poly(2,6-dimethyl-p-phenylene oxide), Polym. J. 35 (2003) 372–378, https://doi.org/10.1295/polymj.35.372.
[51] P.A. Beckmann, C.E. Moore, A.L. Rheingold, Methyl and t-butyl group rotation in a molecular solid: 1H NMR spin-lattice relaxation and X-ray diffraction, Phys. Chem. Chem. Phys. 18 (2016) 1720–1726, https://doi.org/10.1039/C5CP04994F.
[52] F.G. Riddell, M. Rogerson, Intramolecular motions in a series of crystalline benzylammonium bromides and dibenzylamines studied by CP/MAS NMR, J. Chem. Soc. Perkin Trans. 2 (1996) 493–504, https://doi.org/10.1039/P29960000493.
[53] A. Scarperi, E. Carignani, F. Martini, J.P. Embs, J. Wąsicki, G. Barcaro, M. Geppi, A. Pajzderska, Different dynamic behavior of methyl groups in crystalline carbimazole as revealed by a multitechnique experimental and theoretical approach, J. Phys. Chem. C 127 (2023) 5186–5196, https://doi.org/10.1021/acs.jpcc.3c00904.
[54] C.G. Arges, L. Wang, M. Jung, V. Ramani, Mechanically stable poly(arylene ether) anion exchange membranes prepared from commercially available polymers for alkaline electrochemical devices, J. Electrochem. Soc. 162 (2015) F686, https://doi.org/10.1149/2.0361507jes.
[55] R.-A. Becerra-Arciniegas, R. Narducci, G. Ercolani, S. Antonaroli, E. Sgreccia, L. Pasquini, P. Knauth, M.L. Di Vona, Alkaline stability of model anion exchange membranes based on poly(phenylene oxide) (PPO) with grafted quaternary ammonium groups: influence of the functionalization route, Polymer 185 (2019) 121931, https://doi.org/10.1016/j.polymer.2019.121931.
[56] N. Li, T. Yan, Z. Li, T. Thurn-Albrecht, W.H. Binder, Comb-shaped polymers to enhance hydroxide transport in anion exchange membranes, Energy Environ. Sci. 5 (2012) 7888–7892, https://doi.org/10.1039/C2EE22050D.
[57] N. Li, Y. Leng, M.A. Hickner, C.-Y. Wang, Highly stable, anion conductive, comb-shaped copolymers for alkaline fuel cells, J. Am. Chem. Soc. 135 (2013) 10124–10133, https://doi.org/10.1021/ja403671u.

[58] M. Manohar, D. Kim, Enhancement of alkaline conductivity and chemical stability of quaternized poly(2,6-dimethyl-1,4-phenylene oxide) alkaline electrolyte membrane by mild temperature benzyl bromination, RSC Adv. 10 (2020) 36704–36712, https://doi.org/10.1039/D0RA06852G.
[59] D. Gaitanelis, C. Worrall, M. Kazilas, Detecting, characterising and assessing PEEK's and CF-PEEK's thermal degradation in rapid high-temperature processing, Polym. Degrad. Stabil. 204 (2022) 110096, https://doi.org/10.1016/j.polymdegradstab.2022.110096.
[60] M. Day, T. Suprunchuk, J.D. Cooney, D.M. Wiles, Thermal degradation of poly (aryl-ether–ether-ketone) (PEEK): a differential scanning calorimetry study, J. Appl. Polym. Sci. 36 (1988) 1097–1106, https://doi.org/10.1002/app.1988.070360510.
[61] J. Schaefer, E.O. Stejskal, R. Buchdahl, Magic-angle 13C NMR analysis of motion in solid glassy polymers, Macromolecules 10 (1977) 384–405, https://doi.org/10.1021/ma60056a031.
[62] R.J. Wittebort, M.G. Usha, D.J. Ruben, D.E. Wemmer, A. Pines, Observation of molecular reorientation in ice by proton and deuterium magnetic resonance, J. Am. Chem. Soc. 110 (1988) 5668–5671, https://doi.org/10.1021/ja00225a013.
[63] C. Tobar, R. Cordova, T. Solomon, K. Palombo, G. Olivares, J. Helston, W. Luo, D. Cizmeciyan, A. Benesi, Water dynamics in deuterated gypsum, CaSO4·2D2O, investigated by solid state deuterium NMR, J. Magn. Reson. 310 (2020) 106640, https://doi.org/10.1016/j.jmr.2019.106640.
[64] D.I. Kolokolov, I.S. Glaznev, Y.I. Aristov, A.G. Stepanov, H. Jobic, Water dynamics in bulk and dispersed in silica CaCl2 hydrates studied by 2H NMR, J. Phys. Chem. C 112 (2008) 12853–12860, https://doi.org/10.1021/jp801223c.
[65] T.D. Gierke, W.Y. Hsu, The cluster—network model of ion clustering in perfluorosulfonated membranes, in: Perfluorinated Ionomer Membr, American Chemical Society, 1982, pp. 283–307.